Contact Layer as a Propelling Advantage in Throwing

Franck Celestini,[1,†] Joachim Mathiesen,[2] Médéric Argentina,[1] and Christophe Raufaste[1,*]

[1] *Université Côte d'Azur, CNRS, Institut de Physique de Nice, 06100 Nice, France*

[2] *Niels Bohr Institute, University of Copenhagen, Copenhagen, Denmark*

(Received 29 March 2020; revised 21 April 2020; accepted 3 September 2020; published 16 October 2020)

The ability to throw objects is important to hominid evolution and has been central to many technological innovations in human history. The conditions for optimal throwing performance, however, are in general unknown. Here we present ejection experiments of projectiles composed of a rigid and a soft layer. The optimal performance is achieved when the soft layer of the projectiles matches the acceleration dynamics of the throwing engine. Compared with a fully rigid projectile, a bilayered projectile with a small soft elastic layer can achieve a more than 300% increase in translational kinetic energy. Our study emphasizes the importance of not only designing projectiles to optimize the stability in flight, the aerodynamic profile, and the spin, but also to carefully match the mechanical impedance of the projectiles and their thrower.

DOI: 10.1103/PhysRevApplied.14.044026

I. INTRODUCTION

In humans and animals, the release of energy stored inside elastic fibrous structures, like tendons, can produce power outputs far beyond the capability of mere muscles [1]. In fact, elastic tissue structures recoil faster than muscles can shorten, which is used, for example, when jumping [2–5], running [6,7], or throwing [8,9]. The ability to throw objects has offered an evolutionary advantage to primates [10] and in particular humans [11–13], and is tightly coupled to the elasticity of the shoulder [8]. The mechanical work produced in a throw starts with a motion of the hips, is followed by a loading of the elastic elements in the shoulder, and ends with a rapid kinetic energy transfer to the arm and projectile [9]. Underlying these steps, different muscles (in the legs, hips, torso, shoulder, elbow, and wrist) are activated sequentially and the optimal throw happens when the different joints are put into motion with carefully timed delays [14–17]. The timing and activation of successive segments is an active subject of research in the field of robotics, biomechanics, sports, and human evolution [8,9,18–24]. The idea of precise synchronization and timing in throwing is also important in plants and fungi, which use throwinglike mechanisms to release and disperse spores and pollen [25,26]. For example, the sporangia—the spore ejection units in ferns—take advantage of two different time scales to maximize the ejection [27]. Finally, throwing experiments with soft elastic objects have shown that the transfer of energy can be optimized, up to 250%, when the ratio of the time scale of acceleration to the projectile eigenperiod takes a particular value [28].

Inspired by these mechanisms, we design a projectile that delays the release of elastic energy and optimizes the energy transfer within a chain of elastic elements. Specifically, we consider bilayered projectiles thrown by an ejection engine. We show that the throw efficiency of rigid objects, which is generally low, can be drastically improved by more than 300% by adding an extra soft layer between the engine and the rigid object.

II. MATERIALS AND METHODS

A. Ejection setup

The experiments are performed with the ejection engine illustrated in Fig. 1(a). From $t = 0$, the engine plate performs a uniaxial harmonic motion described to a high precision by the function $z_p(t) = A[1 - \cos(2\pi ft)]$. The frequency f of the engine can be varied in the range 20–80 Hz and the amplitude A is approximately 1 mm. Hence, the maximum velocity of the engine, $V_p^* = 2\pi fA$, is around $0.5\,\mathrm{m\,s^{-1}}$ and the maximum acceleration is around $25\,g$, where g is the acceleration of gravity. Moreover, the weights m of the projectiles are negligible relative to the weight of the engine and therefore do not influence the engine motion. We use cylindrical projectiles with a diameter of 12 mm and a length L of 15 mm. The projectiles consist of a soft and a rigid material superposed. The rigid elastic material is made of a hard plastic (polyether ether ketone, Young's modulus $E_r = 3.6$ GPa, and density $\rho_r = 1300\,\mathrm{kg\,m^{-3}}$) and the soft elastic

*christophe.raufaste@unice.fr

†franck.celestini@unice.fr

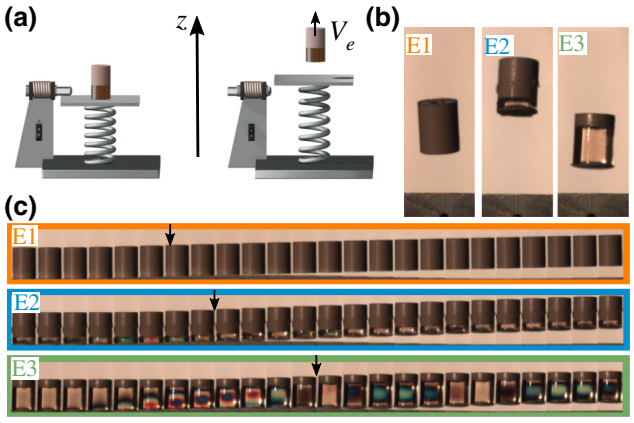

FIG. 1. (a) Basic description of the ejection experiment: initial configuration and takeoff at velocity V_e. (b) Maximal height reached by three projectiles, E1, E2, and E3, with different rigid-soft ratios: fully rigid, a small soft layer, and a large soft layer, respectively. The engine frequency is the same in all cases, $f = 76$ Hz. (c) Image sequences (0.7 ms between images) of these three experiments. For each sequence, an arrow denotes the takeoff time. By using two polarizers, we observed coloring inside the soft material: the photoelastic properties of the hydrogel provided information about the local deformation. The length scale is given by the diameter of the projectiles, 12 mm in all cases. Movies are available in the Supplemental Material [29].

material is made of a gelatin hydrogel ($E_s = 12$ kPa and $\rho_s = 1000\,\mathrm{kg\,m^{-3}}$). Hydrogels are prepared by dissolving gelatin powder (Sigma-Aldrich, gelatin from porcine skin, gel strength 300, type A) in water for 30 min at 80 °C under gentle agitation. The ratio of powder to water is around 15% in mass. In our range of parameters, the hydrogels behave mostly elastically and viscoelastic effects can be neglected. To prepare each projectile, the rigid part is placed at the bottom of a cylindrical mold where the dissolved solution is poured and kept at rest for two hours. Once unmolded, the hydrogel has reticulated and is both elastic and transparent. The contact with the rigid layer is cohesive and prevents the two parts from separating. Gelatin hydrogels are photoelastic, a property exploited to track the local deformation inside the projectiles. The ejection efficiency is quantified after takeoff by the energy transfer factor $\alpha = (V_e/V_p^*)^2$, where V_e is the ejection velocity of the center of mass. This quantity is calculated from the maximal height H of the free flight following complete ejection ($V_e = \sqrt{2gH}$).

We present in Figs. 1(b) and 1(c) the ejection dynamics for three typical projectiles: (E1) a 100% rigid object, (E2) a bilayered object with a small soft layer at the bottom, and (E3) one with a large soft layer at the bottom. For this engine frequency, $f = 76$ Hz, the projectile with the small soft layer is thrown significantly faster—and is ejected higher in consequence—than the purely rigid projectile and the projectile with the large soft layer. An optimum in the soft-rigid ratio is therefore expected. Observing the photoelastic coloring inside the soft layer (Fig. 1), we note that a deformation wave propagates inside this layer, and that elasticity needs to be accounted for to understand the dynamics.

B. Simulations

The experiments are supported by numerical simulations of the deformation dynamics. For the sake of generality, we consider the wave propagation in both the soft and rigid layers. In cylindrical coordinates and assuming axial symmetry of the projectiles, the displacement $\mathbf{u} = (u_r, u_\theta, u_z)$ has the components $u_\theta = 0$, $u_r = u_r(r, z, t)$, and $u_z = u_z(r, z, t)$. We do not expect the longitudinal displacement u_z to depend significantly on the radial coordinate r, so we approximate $u_z(r, z, t) \approx u(z, t)$. The dynamics is therefore driven by the propagation of longitudinal elastic waves inside the projectile. The waves are described by the one-dimensional momentum balance equation

$$\rho(z)\partial_t^2 u(z,t) - \partial_z[E(z)\partial_z u(z,t)] = 0, \tag{1}$$

where z measures the distance from the bottom part of the cylinder along the symmetry axis, $E(z)$ is the local Young modulus, and $\rho(z)$ is the mass density. For our bilayered projectiles, the material parameters are constant in each layer and we recover the classical wave equation with two longitudinal wave velocities, $c_s = \sqrt{E_s/\rho_s}$ and $c_r = \sqrt{E_r/\rho_r}$, inside the soft and rigid layers, respectively. We use the subscripts s and r to denote physical quantities of the soft and rigid materials, respectively. For the numerical simulations, we used a basic semi-implicit (symplectic) Euler finite difference scheme. The point of contact with the plate is assumed to be fully rigid such that the end of the rod upon starting immediately assumes the speed of the plate. The dynamics is subject to the boundary conditions

$$u(0,t) \geq A[1 - \cos(2\pi f t)], \tag{2a}$$

$$u(z,0) = 0 \quad \text{for } z > 0, \tag{2b}$$

$$\partial_t u(z,0) = 0 \quad \text{for } z > 0, \tag{2c}$$

$$\partial_z u(z,t) \overset{z\to L}{\to} 0. \tag{2d}$$

In our simulations, the projectile is released from the throwing engine as soon as the strain crosses from positive to negative at $z = 0$. Note that it is possible for a projectile to reconnect to the engine after takeoff, that is, the engine can catch up with the trailing edge and thereby result in successive stages of ejection and reconnection.

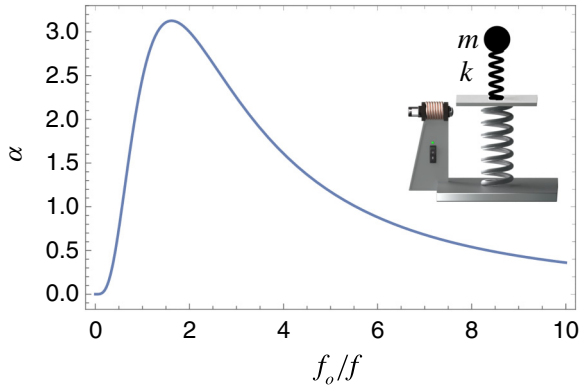

FIG. 2. Energy transfer factor α for the spring-mass model. This function α reaches 3.13 for $f_0/f = 1.62$.

C. Spring-mass model

We derive here the results obtained with a simple spring-mass projectile—a point mass m on top of a massless spring of stiffness k and free length L—to give insights about the role of inertia and elasticity in throwing experiments. This system has an eigenfrequency $f_0 = (1/2\pi)\sqrt{k/m}$. We denote by z_m the position of the point mass:

$$\ddot{z}_m = -(2\pi f_0)^2(z_m - z_p - L). \tag{3}$$

Here $z_p = A[1 - \cos(2\pi ft)]$ measures the position of the engine plate. The solution of this forced harmonic oscillator equation, with $z_m(0) = L$, is

$$z_m(t) = L + A + \frac{A}{f^2 - f_0^2}[f_0^2\cos(2\pi ft) - f^2\cos(2\pi f_0 t)]. \tag{4}$$

The projectile takes off when $z_m - z_p = L$, at time $t_e = 1/(f + f_0)$. The velocity ratio at takeoff V_e/V_p^* is predicted to be

$$V_e/V_p^* = \frac{\dot{z}_m(t_e)}{2\pi fA} = \frac{f_0/f}{f_0/f - 1}\sin\left(\frac{2\pi}{f_0/f + 1}\right). \tag{5}$$

In Fig. 2, we show that the energy transfer factor $\alpha = (V_e/V_p^*)^2$ reaches the maximum 3.13 for $f_0/f \simeq 1.62$. We interpret that this peak efficiency results from a particular match between the acceleration time of the engine (proportional to $1/f$) and the typical time of the projectile deformation (proportional to $1/f_0$). Finally, we point out that this projectile has a maximum energy transfer factor 3.13, even higher than the maximal value 2.5 obtained with a homogeneous linear projectile [28].

III. RESULTS

We study configurations where the rigid layer is on top and where the soft layer is on top, and we vary the ratio $x = L_s/L$ between the length of the soft layer L_s and the projectile length L.

A. Rigid-on-top configuration

We first consider the rigid-on-top configuration. In Figs. 3(a) and 3(b) we present the height reached by various projectiles for $c_s = 3.4$ m s^{-1}, for several x values and two different engine frequencies, 34 and 76 Hz, leading to ratios c_s/Lf equal to 6.5 and 2.9, respectively. In all cases, there is a very good agreement between the experiments and simulations. For both frequencies, the expected rigid behavior, $\alpha = 1$, is recovered when x equals 0. For intermediate values of x, we observe a peak in the energy

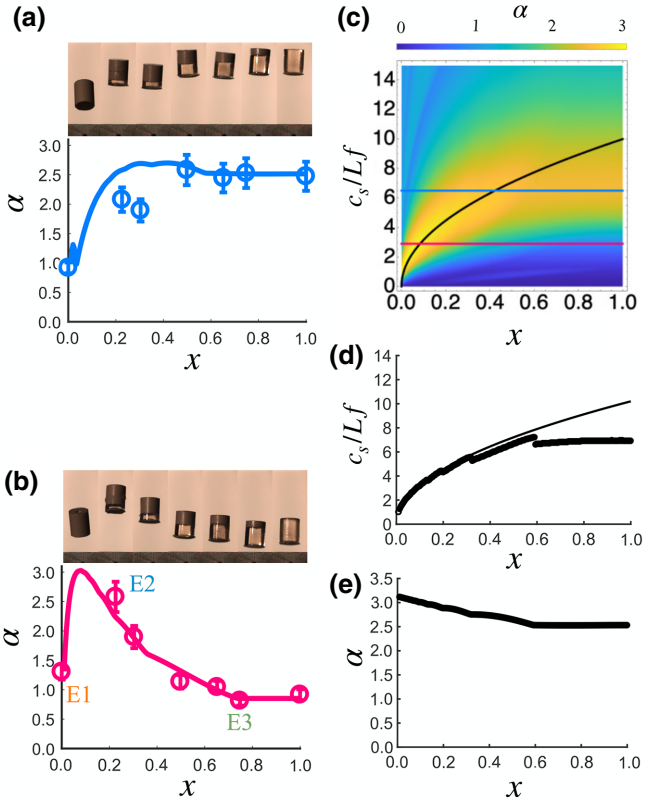

FIG. 3. Ejection of projectiles with a rigid top layer. We show the energy transfer factor α as a function of the soft ratio x for the engine frequencies 34 and 76 Hz in (a) and (b), respectively. Images of the maximal heights are displayed for each case. The experimental measurements are shown with symbols, while the numerical predictions are represented by solid curves. E1, E2, and E3 refer to Fig. 1. (c) Color plot of α as a function of c_s/Lf and x (color scale displayed on the right), deduced from the numerical model. The particular values of c_s/Lf, 2.9 from (a) and 6.5 from (b), are represented by horizontal lines (using the color scheme of the two cases). The dark solid curves shown in (c) and (d) correspond to the model $c_s/Lf = 10.2\sqrt{x}$. (d) The ratio c_s/Lf as a function of x for the maximal α value found along a vertical line in the α diagram (c). (e) Maximal α value as a function of x.

transfer factor. It is particularly pronounced for $c_s/Lf = 2.9$. In this case, α reaches values close to 3 for both the simulations and experiments.

The existence of optima in α is examined systematically with simulations, by varying the values of c_s/Lf and x in Eq. (1), and we present the results of this analysis in Figs. 3(c)–3(e). We note the existence of a best ejection performance region with $\alpha \sim 3.1$, which follows the curve $c_s/Lf \sim 10\sqrt{x}$, from $x = 0$ until $x \sim 0.3$.

This maximal value reminds $\alpha = 3.13$ obtained with the spring-mass model in Sec. II C and we propose insights about this peculiar behavior: if the rigid part is assumed infinitely rigid, the system can be described by a single spring-mass system of mass $m \sim SL\rho$ (the total mass) and of spring stiffness $k = SE_s/L_s = SE_s/xL$ (the value of the soft part only), with S the area of the projectile cross section. Following the definition of $f_0 = (1/2\pi)\sqrt{k/m} = c_s/2\pi L\sqrt{x}$ and the highest efficiency found for $f_0/f = 1.62$, we deduce that the position of the "optimal crest" can be determined from $c_s/Lf = 1.62\ 2\pi\sqrt{x} = 10.2\sqrt{x}$, which gives a perfect match with respect to the predictions of the continuous model, as presented in Figs. 3(c) and 3(d). The quasistatic assumption that the elasticity of the soft part can be accounted by an ideal homogeneous spring requires that the typical time of the ejection (proportional to $1/f$) is significantly larger than the propagation time in the soft layer (proportional to xL/c_s). In the vicinity of the optimal ejection, $f \sim f_0 \sim (c_s/L)(1/\sqrt{x})$ and the condition becomes $\sqrt{x} \ll 1$, or simply $x \ll 1$. This is consistent with experiment E2 in Fig. 1(c): the small soft layer seems to be deformed homogeneously as attested by the uniform coloring.

In the Appendix, we demonstrate that we need to add the condition $E_s/E_r \ll x$ to account for the finite rigidity of the top part and distinguish between $x = 0$ and the limit $x \to 0$. Given the values of E_s/E_r (typically 10^{-6} in our experiments), this moderately thin soft layer limit $E_s/E_r \ll x \ll 1$, hereafter referred to as $x \to 0$, is singular and differs from the rigid case $x = 0$: this system gives a best ejection $\alpha = 3.13$ for $c_s/Lf = 10.2\sqrt{x}$, in very good agreement with the simulations. The case in which $x = 0$ implies that α equals 1, as expected, because the projectile can be considered as rigid. The limit $x \to 0$ is of particular interest, because we show that the addition of a thin soft layer can lead to very efficient ejection if the layer properties match the dynamics of the catapult. For larger values of x, the crest follows $c_s/Lf = 6.8$ and α tends to 2.5, as shown in Figs. 3(d) and 3(e); the limit $x = 1$ recovers the results obtained with a soft homogeneous material [28].

B. Soft-on-top configuration

The soft-on-top configuration results are shown in Fig. 4. Clearly, the ejection performances are lower than in the previous case: the heights reached by these projectiles are notably smaller than the rigid-on-top experiments, for the two frequencies of the ejection engine, as shown in Figs. 4(a) and 4(b). For $c_s/Lf = 6.5$ [see Fig. 4(a)], there is a smooth transition in the transfer factor from a rigid object ($x = 0$) to a soft homogeneous projectile ($x = 1$), and the highest values in α are reached near $x = 1$, that is, for soft homogeneous projectiles. In Fig. 4(b) we show that, in the case $c_s/Lf = 2.9$, there is no clear advantage in using a bilayered projectile over a homogeneous projectile. In order to search the parameter space for the best ejection, we show in Figs. 4(c)–4(e) the numerical predictions of the model, and it appears that the best factor α is reached for $x = 1$ (i.e., a soft homogeneous projectile). The soft-on-top configuration [Figs. 4(c) and 4(d)] seems systematically less efficient than the rigid-on-top configuration [Figs. 3(c) and 3(d)].

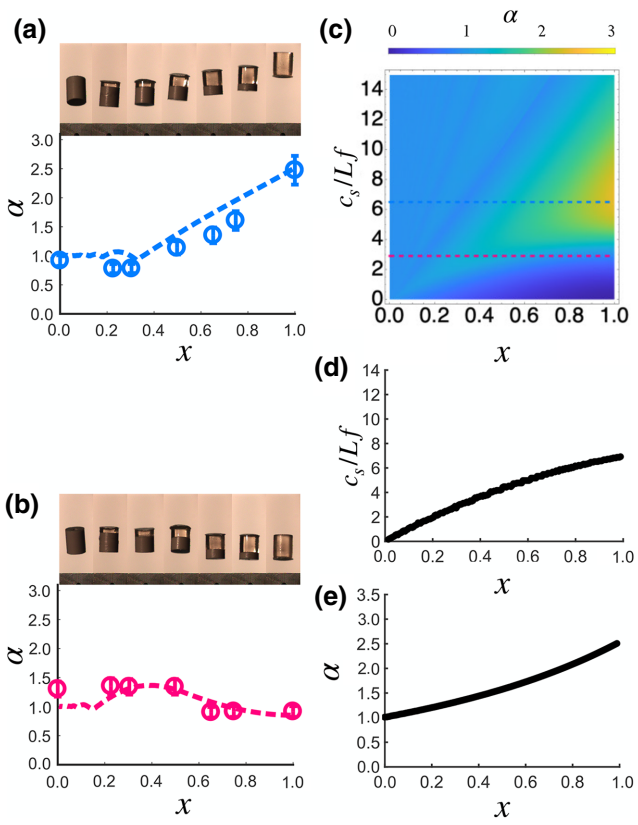

FIG. 4. Ejection of projectiles with a soft top layer. We plot α vs x for the engine frequencies 34 and 76 Hz in (a) and (b), respectively. Images of the maximal heights are displayed for each case. The experimental measurements are shown with symbols, while the numerical predictions are represented by dashed curves. (c) Color plot of α as a function of c_s/Lf and x (color scale displayed on top), deduced from the numerical model. The particular values of c_s/Lf , 2.9 from (a) and 6.5 from (b), are represented by horizontal lines (using the color scheme of the two cases). (d) The ratio c_s/Lf as a function of x for the maximal α value found along a vertical line in the α diagram (c). (e) Maximal α value as a function of x.

C. An optimal dynamics

To summarize, rigid projectiles designed with an additional soft layer at their trailing edge exhibit an "optimal crest" that gives an optimal value for α, whatever the value of x, if c_s/Lf is adjusted correctly; it lies in the range $\alpha = 3.1$ for $x \to 0$ to $\alpha = 2.5$ for $x = 1$.

In terms of the dynamics, optimal ejection is provided by a tuned delayed response of the soft layer. To illustrate this idea, we compare in Fig. 5 the temporal evolution of the relevant quantities during the ejection of a rigid projectile (a) and an optimal bilayered projectile (b) given by the spring-mass model with $f_0/f = 1.62$ (Sec. II C). During the takeoff, the duration of the contact of the projectile with the plate is greatly enhanced in (b) with respect to (a). In the rigid case, the contact force F decreases from an initial maximum towards zero as the plate reaches its maximum velocity V_p^*. In addition, the maximal force exerted onto the projectile is greater in (b) than in (a). Since the transfer of energy from the plate to the projectile is given by $\int_0^{te} F(t)\dot{z}_p(t)dt$, where $\dot{z}_p(t) = 2\pi Af \sin(2\pi ft)$ is the plate velocity and $F(t)\dot{z}_p(t)$ is the instantaneous mechanical power, we infer that the rigid case cannot be optimal since the contact force and the plate velocity are never maximal at the same time. In contrast, the bilayered projectile delays the release of elastic energy and has a contact force in phase with the plate velocity, which ensures an optimal transfer. The nature of the contact force is the key element to discriminate projectiles. If we imagine an ideal engine that could prescribe the same time-dependent force instead of a prescribed engine plate displacement, the motion would be directly dictated by Newton's second law and the ejection velocity would be identical whatever the projectile.

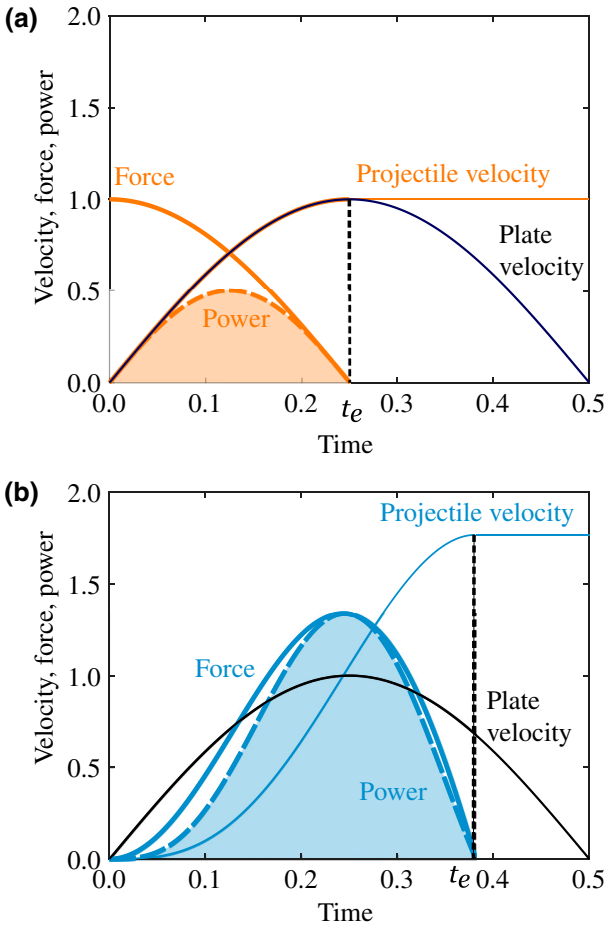

FIG. 5. Temporal evolution of the plate (thin black curves) and projectile velocities (thin colored curves), the contact force (thick curves), and the power (dashed curves) for a rigid projectile (a) and an optimal bilayered projectile (b). The energy transferred to the projectiles is represented by the area underneath the power curve. Dimensionless quantities are represented and velocity, force, and time are divided by $2\pi Af$, $mA(2\pi f)^2$, and $1/f$, respectively.

IV. DISCUSSION

In the light of the results, we can discuss the relevance of such projectiles for human throwing. Following Cross [30], the total kinetic energy provided by our body for an overarm throw is only partially transferred to the (rigid) projectile. In fact, segments of our arm, which can be equated with the throwing engine in our study, are still in motion once the projectile is ejected. Assuming that these segments move with the same velocity as that of the projectile, the throw efficiency (defined here as the ratio of the projectile kinetic energy to the kinetic energy provided by our body) is a function of the mass ratio m/M, where m is the mass of the projectile and M the equivalent mass of the throwing engine, which corresponds roughly to the mass of the forearm and hand, typically $M = 1$–2 kg [30]. In the case of heavy projectiles, such as shot put, when $m/M \gg 1$, the thrower can mobilize most of the kinetic energy for the projectile and the efficiency is close to 1. Conversely, for $m/M \ll 1$, this mode of propulsion becomes ineffective and most of the kinetic energy remains inside our body, leading to potential injuries. This could explain the difference between baseball and (American) football overarm throws. Both have very similar throwing sequences, but the difference in the mass of the balls, 140–150 and 400–430 g, respectively, is significant and makes the baseball pitcher more susceptible to injury than his football counterpart [31]. In the same vein, Cohen and Clanet [32] have shown that the mode of propulsion for ball sports (throwing versus hitting) correlates strongly with the mass ratio between the ball and the throwing instrument, which in light of our results can be explained by a pursuit of the maximum energy transfer rate.

Actually, we can experience the effect ourselves with two more extreme throwing examples: try to perform an overarm throw with a golf ball and a handball, 45 and 450 g, respectively, as fast as you can. The throw with the heaviest ball feels smooth, while in the other case you have

a frustrated impression that you cannot mobilize all your strength and that your arm gets overstretched.

Our study is particularly relevant for the inefficient limit $m/M \ll 1$, since the motion of the throwing engine is not influenced by the mass of the projectile, and we see a huge potential in designing projectiles to delay the release of elastic energy and increase the energy transfer by 300%. As a real-life example, we could imagine adding a homogeneous spring, with spring constant k, at the trailing edge of the (rigid) golf ball to increase its throw efficiency. Our study predicts that the peak efficiency is reached when $\sqrt{k/m} = 10.2f$ (Sec. II C). With a typical throw time $1/f \sim 1\,\mathrm{s}$, this leads to $k \sim 5\ \mathrm{N\,m^{-1}}$. For heavy objects, we would not expect a large difference in the efficiency of rigid and time-delayed projectiles, although a slight optimization of a few percent may still be relevant in the context of competition.

Finally, it is currently being debated how to regulate footwear in road running [33]. For example, footwear can be optimized to not only conserve energy but also to time the energy release from the sole according to the characteristics of the individual runner. To ensure fairness, it has been proposed to regulate the thickness of the sole [33], and thereby reduce the number of parameters one can use for optimization during the technological development. However, our experiments show [see, for example, Fig. 3(c)] that a limitation on the thickness of the soft layer can potentially be compensated for by a change in the elastic properties.

V. CONCLUSION

By modifying the mechanical properties of a projectile, the throw efficiency can be significantly changed. For optimal throws, the key point is to delay the reaction force experienced at the thrower-projectile contact such that the contact force and velocity are in phase during the propulsive phase, thereby maximizing the mechanical power. For a homogeneous projectile or a spring-mass system, this is obtained by matching the throwing time with the eigenperiod of the projectile oscillations. For a bilayered projectile, there is an optimum if the soft part is placed at the trailing edge. In this case, the gain in translation energy is a factor of three larger than for a rigid projectile. From an engineering point of view, massive propulsion engines are not the best choice to propel light projectiles. Actually, the lower the mass of the projectile, the lower the mass of the throwing instrument should be, in order to achieve the best efficiency. If the mass cannot be adjusted, projectiles designed for elastic-assisted throwing seem to be a very good option.

ACKNOWLEDGMENTS

We thank Fabrice Mortessagne for his support of the project, and acknowledge the financial support of CNRS. F.C. and C.R. thank Lorenzo Betti and Nicolas David for their input at the beginning of the project.

APPENDIX: DOUBLE SPRING-MASS MODEL

We model each part of the bilayered projectile with a spring-mass system, as depicted in Fig. 6. We approximate the upper part of the projectile with a point mass m_t, located at $z = z_t$, and the bottom part with a point mass m_b, which is located at $z = z_b$. These two components are connected together with a spring of stiffness k_t and length l_t. The engine is modeled through a plate, located at $z = z_p(t)$, which triggers the bottom mass through an elastic spring of stiffness k_b and length l_b. The dynamics of this model is described by

$$\begin{aligned} m_t\ddot{z}_t &= k_t(z_t - z_b - l_t), \\ m_b\ddot{z}_b &= -k_t(z_t - z_b - l_t) - k_b(z_b - z_p - l_b), \\ z_p &= A[1 - \cos(\omega t)]. \end{aligned}$$

We have neglected the effect of gravity.

To mimic the continuous medium, we approximate the spring response to the elastic force resulting from a length change in the bulk; hence, $k_{t,b} = SE_{t,b}/l_{t,b}$, where $E_{t,b}$ represents the Young modulus of the material of the upper and bottom parts of the projectile, and S is the transverse area of the projectile. We assume that $l_t = (1 - r)L$, and $l_b = rL$, as well as $m_t = m(1 - r)$ and $m_b = rm$, where m and L are respectively the mass and the length of the projectile. The variable r measures the composition of the projectile: $r = 0$ corresponds to a homogeneous object with a Young

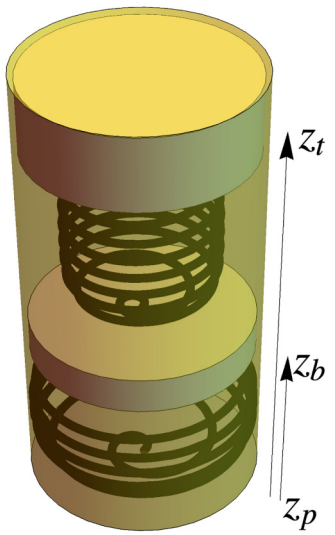

FIG. 6. Schematic representation of the double spring-mass model. Two masses located at z_t and z_b interact with one spring of stiffness k_t. The bottom mass is connected to the moving plate with a spring of stiffness k_b. The plate position is z_p.

modulus equal to E_t, while $r = 1$ corresponds to a homogeneous object with a Young modulus equal to E_b. The above system can be rewritten in terms of this ratio parameter, i.e.,

$$(1-r)\ddot{z}_t = -\omega_t^2 \frac{1}{1-r}(z_t - z_b - l_t), \tag{A1}$$

$$r\ddot{z}_b = \omega_t^2 \frac{1}{1-r}(z_t - z_b - l_t) - \omega_b^2 \frac{1}{r}(z_b - z_p - l_b), \tag{A2}$$

where we have introduced $\omega_{t,b}^2 = SE_{t,b}/ml_{t,b}$. Initially, both masses are at equilibrium: $z_t(0) = l_b + l_t$ and $z_b(0) = l_b$. The projectile will takeoff from the forcing plate at time $t = t_e$, for which $z_b(t_e) - z_p(t_e) = l_b$.

We first study the dynamics of a soft homogeneous projectile. This configuration is reached as r tends to 1 (the case r tends to 0 will be discussed later). The inertia of the top mass is neglected and z_t follows z_b adiabatically from Eq. (A1): $z_t = z_b$ as $l_t \to 0$. In this limit, we recover the dynamics described by the single spring-mass model where ω_0 is now ω_b. Hence, our model predicts an efficiency peak in the energy transfer factor for a homogeneous soft projectile. Nevertheless, the agreement remains qualitative, since the continuous model anticipates 2.5 as the highest value for α.

We now study the ejection dynamics of bilayered projectiles. For a composite projectile with very different Young's moduli, there is a general solution:

$$z_t(\omega t) = l_b + l_t + A[1 - (Z_{1t} + Z_{2t})\cos\omega t - (1 - Z_{1t})\cos\omega_1 t - (1 - Z_{2t})\cos\omega_2 t], \tag{A3}$$

$$z_b(\omega t) = l_b + A[1 - (Z_{1b} + Z_{2b})\cos\omega t - (1 - Z_{1b})\cos\omega_1 t - (1 - Z_{2b})\cos\omega_2 t]. \tag{A4}$$

This solution takes into account the driving of the moving plate and also the two vibration modes of the system. The frequencies and the amplitudes of the modes are respectively denoted by $\omega_{1,2}$, $Z_{1,2t}$, and $Z_{1,2b}$. We study the dynamics of bilayered projectiles for which one of the materials is supposed to be much more rigid than the other material (i.e., either $\omega_t \ll \omega_b$ or $\omega_b \ll \omega_t$): in this limit one of the two eigenfrequencies $\omega_{1,2}$ is much higher than the other eigenfrequency. Let us assume that $\omega_1 \ll \omega_2$: the effect of the associated eigenmode will be small, and we can show that $Z_{2t,b} \ll Z_{1t,b}$. The dynamics of the bottom part becomes

$$z_b(t) = l_b + A[1 - Z_{1b}\cos(\omega t) - (1 - Z_{1b})\cos(\omega_1 t)],$$

which is very similar to those of z_m in the single spring-mass model, except that the angular frequency ω_1 depends on ω_b, ω_t, and x. This expression predicts the takeoff time

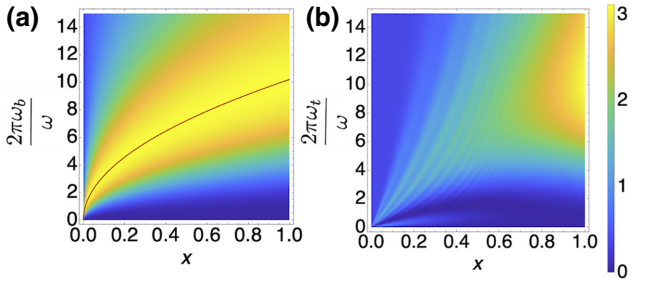

FIG. 7. Energy transfer factor α for a bilayered projectile, deduced from the double spring-mass model. (a) The bottom part is soft. (b) The upper part is soft.

$t_e = 2\pi/(\omega + \omega_1)$, and we can compute the energy transfer factor α, whose functional shape is exactly the same as the single spring-mass model.

In Figs. 7(a) and 7(b), we summarize the behavior of α as a function of the control parameters for projectiles composed of a soft bottom material and a soft top material, respectively. By comparing the results presented in Fig. 3c and 4c, we conclude that the simple model predicts qualitatively the super propulsive regions in the dimensionless parameter space, namely near $x = 1$, for both configurations, and the square-root-like crest for the rigid-on-top projectiles.

For a very thin bottom layer, r tends to 0, as does the bottom mass: z_b will follow z_t adiabatically in (A2) and the model reduces to

$$\ddot{z}_t + \frac{\omega_t^2\omega_b^2}{\omega_b^2 + r\omega_t^2}(z_t - z_p - L) = 0, \tag{A5}$$

$$z_b = \frac{\omega_b^2}{\omega_b^2 + x\omega_t^2} z_p + \frac{x\omega_t^2}{\omega_b^2 + x\omega_t^2} z_t. \tag{A6}$$

For projectiles with the soft part at the top, $\omega_t = \omega_0$ and $\omega_b^2 \gg r\omega_0^2$: the dynamics of the bottom layer simplifies to

$$\ddot{z}_t + \omega_0^2(z_t - z_p - L) = 0.$$

This corresponds to the limit of the single spring-mass model, and justifies the existence of a maximum in the transfer factor near $x = 1$ and $2\pi\omega_0/\omega \sim 10.2$ [see Fig. 7(b)], because we have seen that the most efficient ejection for the single spring-mass model is obtained for $\omega_0/\omega \sim 1.62$.

If the bottom layer is soft, there are two possible behaviors. For an extremely thin layer $r \ll \omega_b^2/\omega_t^2$, the system behaves as

$$\ddot{z}_t + \omega_t^2(z_t - z_p - L) = 0,$$

and the projectile can be considered as homogeneous and rigid. Hence, if $x = r \ll \omega_b^2/\omega_t^2$, the transfer factor is equal to 1, as seen in Fig. 7(a), at $x = 0$. There exists the

particularly interesting limit $\omega_b^2/\omega_t^2 \ll x \ll 1$, for which the dynamics of the projectile obeys the equation

$$\ddot{z}_t + \frac{\omega_b^2}{x}(z_t - z_p - L) = 0.$$

Consequently, for a moderately thin soft bottom layer, the bilayered projectile behaves as a single spring-mass model with frequency $\omega_b/\sqrt{x}$. Hence, the projectile will be best propelled if $\omega_b = 1.62\omega\sqrt{x}$, which explains the existence of the crest in the continuous model. This square root agrees qualitatively well for both the simple model (see Fig. 7) and the continuous approach (see Fig. 3). Consequently, for a rigid object with a Young modulus E_r, attaching a soft material with Young's modulus E_s of thickness higher than $(E_s/E_r)L$ will achieve the best ejection performance.

[1] G. J. Ettema, Mechanical efficiency and efficiency of storage and release of series elastic energy in skeletal muscle during stretch-shorten cycles, J. Exp. Biol. **199**, 1983 (1996).

[2] R. L. Marsh and H. B. John-Alder, Jumping performance of hylid frogs measured with high-speed cine film, J. Exp. Biol. **188**, 131 (1994).

[3] K. Kubo, Y. Kawakami, and T. Fukunaga, Influence of elastic properties of tendon structures on jump performance in humans, J. Appl. Physiol. **87**, 2090 (1999).

[4] M. Burrows, Froghopper insects leap to new heights, Nature **424**, 509 (2003).

[5] H. C. Astley and T. J. Roberts, Evidence for a vertebrate catapult: Elastic energy storage in the plantaris tendon during frog jumping, Biol. Lett. **8**, 386 (2012).

[6] T. J. Roberts, R. L. Marsh, P. G. Weyand, and C. R. Taylor, Muscular force in running turkeys: The economy of minimizing work, Science **275**, 1113 (1997).

[7] A. M. Wilson, J. C. Watson, and G. A. Lichtwark, A catapult action for rapid limb protraction, Nature **421**, 35 (2003).

[8] N. T. Roach, M. Venkadesan, M. J. Rainbow, and D. E. Lieberman, Elastic energy storage in the shoulder and the evolution of high-speed throwing in homo, Nature **498**, 483 (2013).

[9] N. T. Roach and D. E. Lieberman, Upper body contributions to power generation during rapid, overhand throwing in humans, J. Exp. Biol. **217**, 2139 (2014).

[10] W. H. Calvin, Did throwing stones shape hominid brain evolution? Ethol. Sociobiol. **3**, 115 (1982).

[11] J. Goodall, Tool-using and aimed throwing in a community of free-living chimpanzees, Nature **201**, 1264 (1964).

[12] W. J. Hamilton III, R. E. Buskirk, and W. H. Buskirk, Defensive stoning by baboons, Nature **256**, 488 (1975).

[13] G. Westergaard, C. Liv, M. Haynie, and S. Suomi, A comparative study of aimed throwing by monkeys and humans, Neuropsychologia **38**, 1511 (2000).

[14] H. J. J. Jöris, A. J. Edwards van Muyen, G. J. van Ingen Schenau, and H. C. G. Kemper, Force, velocity and energy flow during the overarm throw in female handball players, J. Biomech. **18**, 409 (1985).

[15] R. M. Alexander, Optimum timing of muscle activation for simple models of throwing, J. Theor. Biol. **150**, 349 (1991).

[16] C. A. Putnam, Sequential motions of body segments in striking and throwing skills: Descriptions and explanations, J. Biomech. **26**, 125 (1993).

[17] M. Hirashima, H. Kadota, S. Sakurai, K. Kudo, and T. Ohtsuki, Sequential muscle activity and its functional role in the upper extremity and trunk during overarm throwing, J. Sports Sci. **20**, 301 (2002).

[18] M. Grebenstein, M. Chalon, W. Friedl, S. Haddadin, T. Wimböck, G. Hirzinger, and R. Siegwart, The hand of the DLR hand arm system: Designed for interaction, Int. J. Robot. Res. **31**, 1531 (2012).

[19] D. Braun, M. Howard, and S. Vijayakumar, Optimal variable stiffness control: Formulation and application to explosive movement tasks, Auton. Robot. **33**, 237 (2012).

[20] E. M. Williams, A. D. Gordon, and B. G. Richmond, Biomechanical strategies for accuracy and force generation during stone tool production, J. Hum. Evol. **72**, 52 (2014).

[21] H. Liu, S. Leigh, and B. Yu, Comparison of sequence of trunk and arm motions between short and long official distance groups in javelin throwing, Sports Biomech. **13**, 17 (2014).

[22] B. Serrien, R. Clijsen, J. Blondeel, M. Goossens, and J.-P. Baeyens, Differences in ball speed and three-dimensional kinematics between male and female handball players during a standing throw with run-up, BMC Sports Sci. Med. Rehabilitation **7**, 27 (2015).

[23] D. W. Haldane, M. M. Plecnik, J. K. Yim, and R. S. Fearing, Robotic vertical jumping agility via series-elastic power modulation, Sci. Robot. **1**, eaag2048 (2016).

[24] P. Fasbender, T. J. Korff, V. B. Baltzopoulos, and N. P. Linthorne, Optimal mass of the arm segments in throwing: A two-dimensional computer simulation study, Eur. J. Sport Sci. 1 (2020).

[25] Y. Forterre, Slow, fast and furious: Understanding the physics of plant movements, J. Exp. Bot. **64**, 4745 (2013).

[26] A. Sakes, M. v. d. Wiel, P. W. J. Henselmans, J. L. v. Leeuwen, D. Dodou, and P. Breedveld, Shooting mechanisms in nature: A systematic review, PLoS ONE **11**, e0158277 (2016).

[27] X. Noblin, N. O. Rojas, J. Westbrook, C. Llorens, M. Argentina, and J. Dumais, The fern sporangium: A unique catapult, Science **335**, 1322 (2012).

[28] C. Raufaste, G. R. Chagas, T. Darmanin, C. Claudet, F. Guittard, and F. Celestini, Superpropulsion of Droplets and Soft Elastic Solids, Phys. Rev. Lett. **119**, 108001 (2017).

[29] See Supplemental Material at http://link.aps.org/supplemental/10.1103/PhysRevApplied.14.044026 for videos.

[30] R. Cross, Physics of overarm throwing, Am. J. Phys. **72**, 305 (2004).

[31] K. Meister, Injuries to the shoulder in the throwing athlete: Part one: Biomechanics/Pathophysiology/Classification of injury, Am. J. Sports Med. **28**, 265 (2000).

[32] C. Cohen and C. Clanet, Physics of ball sports, Europhys. News **47**, 13 (2016).

[33] G. T. Burns and N. Tam, Is it the shoes? A simple proposal for regulating footwear in road running, Br. J. Sports Med. **54**, 439 (2019).